Int. J Multiphase Flow Vol 12, No 4, pp 543–558, 1986
Printed in Great Britain

0301-9322/86 $3.00+.00
Pergamon Journals/Elsevier

FLOODING IN AN ELBOW BETWEEN A VERTICAL AND A HORIZONTAL OR NEAR-HORIZONTAL PIPE

PART II: THEORY

K. H. ARDRON
Thermalhydraulics Research Branch, Whiteshell Nuclear Research Establishment, Atomic Energy of Canada Limited, Pinawa, Manitoba ROE 1LO, Canada

and

S. BANERJEE
Department of Chemical and Nuclear Engineering, University of California, Santa Barbara, CA 93106, U.S.A.

(*Received* 6 *September* 1984; *in revised form* 20 *October* 1985)

Abstract—This is the second of two papers on countercurrent gas–liquid flow flooding in an elbow of which the upper limb is vertical and the lower limb is horizontal or slightly inclined. In part I, experiments were described in which flooding limits were measured in air–water flow in various pipe elbows of this type; flooding was found to be caused by the onset of slugging at a hydraulic jump which formed in the lower limb of the elbow close to the bend. In the present paper a theoretical model is developed by which the flooding limits for this elbow geometry can be predicted. The model assumes that a smooth stratified flow exists in the lower limb of the elbow, with a free outfall at the exit. Flooding is assumed to coincide with slug formation just downstream of the bend where the liquid depth is greatest. The model gives a reasonable prediction of the observed effects on the flooding limit of the length-to-diameter ratio and angle of inclination of the lower leg of the elbow.

1. INTRODUCTION

In a previous paper (Siddiqui *et al.* 1986), referred to subsequently as part I, experiments were described in which flooding limits were measured for air–water flow in elbows formed by vertical and horizontal or near-horizontal pipes. The main observations were that:

(i) flooding in the elbow geometry occurred at gas flow rates much smaller than those needed to produce flooding in a vertical pipe of equal diameter;
(ii) flooding inception coincided with unstable wave formation (slugging) in the lower leg of the elbow, close to the bend;
(iii) the gas flow rate for flooding depended strongly on the length-to-diameter ratio and inclination of the lower leg of the elbow, and on the radius of curvature of the bend.

In this paper a theoretical model is described which provides a convenient method for predicting the flooding limit in an elbow between a vertical and a horizontal or near-horizontal pipe. The analysis is based on the fundamental assumption that flooding is due to the onset of slugging in the lower leg of the elbow close to the bend, where the liquid depth is greatest. The gas and liquid flow rates at the flooding point are calculated by solving the phasic mass and momentum conservation equations for the stratified two-phase flow in the lower limb of the elbow.

Gardner (1983) recently developed a model for flooding in a horizontal pipe by considering the motion of lossless waves in a stratified flow. However, when applied to the case of a 90° vertical-to-horizontal elbow, his model does not describe the observed effect of the horizontal pipe length-to-diameter ratio on the flooding limit; nor is the effect of pipe inclination accounted for. More importantly, Gardner's model predicts that the flow rate for zero liquid downflow (i.e. complete liquid carry-up) is similar for horizontal and vertical tubes. This is inconsistent with experimental observations, which show that the gas flow rate needed to prevent liquid penetration into a 90° elbow can be four or five times smaller than that for the equivalent vertical tube. The model described in the present paper predicts the geometrical trends, and the limit for complete carry-up, with reasonable accuracy.

2 DESCRIPTION OF THE PHENOMENA

The situation of interest is shown in figure 1. A long tube inclined at an angle ϕ to the horizontal (a positive value of ϕ will be used to denote an upward inclination) is connected at inlet to a vertical tube by an elbow. Liquid at a constant flow rate is introduced into the vertical leg at A through a T-piece or porous sinter, etc. (not shown) and gas at a constant flow rate is introduced at the tube exit E. The liquid flows down the vertical tube as a wall film, and then forms a stratified flow in the lower limb of the elbow

We assume that the velocity of the liquid stream entering the lower limb of the elbow from the bend at B is initially supercritical (i.e. above the velocity of propagation of gravity waves). A transition to subcritical flow is assumed to take place at a hydraulic jump at C, which is the point of maximum liquid depth. A free out-fall is assumed at E, implying that the liquid velocity at E is equal to the critical velocity (Chow 1959). Between C and E the liquid depth steadily decreases while the liquid velocity increases.

In the experiments described in part I the above situation was observed experimentally. It was observed that as the air flow was increased the hydraulic jump moved close to the elbow B. When the air flow rate reached a critical value, unstable wave formation (slugging) occurred at the crest of the hydraulic jump, where the air velocity was highest, leading to expulsion of water from the tube inlet (flooding). Thus, for the flow geometry shown in figure 1, flooding is identified with the inception of a wave instability at a hydraulic jump located in the lower leg of the elbow close to the bend.

3. THEORY

To predict the gas and liquid flow rate at the flooding point for the geometry in figure 1 we assume, as described above, that flooding coincides with the onset of slugging at the hydraulic jump located at point C close to the pipe bend. The gas flow rate at slugging is related to the height of the jump by the purely empirical equation given in part I. A second equation is provided by the condition that the liquid velocity at the exit E is equal to the critical velocity. Finally the conditions at B and E are related by solving the conservation equations for a stratified flow between B and E using a two-fluid formulation. In summary, therefore, the flooding curve is calculated from a theoretical analysis of near-horizontal stratified flow coupled with a purely empirical correlation for the onset of slugging at the hydraulic jump. Details are described below.

3.1 Instability criterion

It was observed experimentally in part I that the onset of slugging at the hydraulic jump near the pipe bend could be described using the equation

$$j_G^* = j_{Gc}^* \alpha_G^{3/2}, \qquad [1]$$

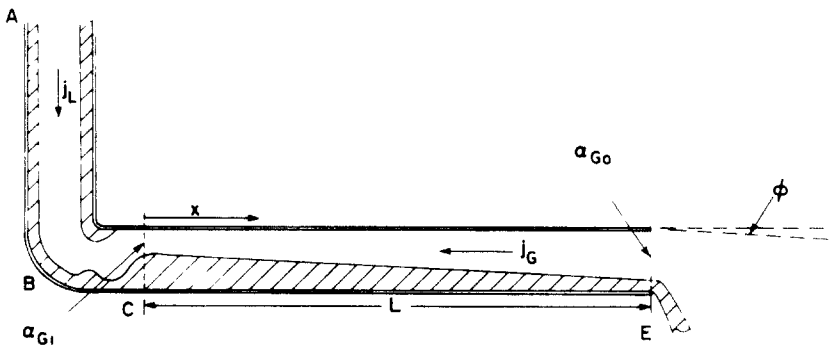

Figure 1 Flow system under consideration

where j_k^* is the nondimensional volumetric flux of phase k defined by

$$j_k^* = \frac{\alpha_k u_k}{(gD\rho_{LG}/\rho_k)^{1/2}}. \qquad [2]$$

Here α_k, ρ_k, and u_k are, respectively, the volumetric concentration, density, and actual velocity of phase k ($k = G$ denotes the gas phase and $k = L$ denotes the liquid phase). g and D are the acceleration due to gravity and the pipe diameter, respectively, and $\rho_{LG} = \rho_L - \rho_G$.

In [1], the factor j_{Gc}^* is a constant, which was found experimentally to be approximately equal to 0.2; α_G denotes the void fraction at the location of the hydraulic jump, where the liquid depth is greatest.

3.2 Calculation of the stratified flow

We consider the horizontal stratified countercurrent flow in the lower limb BE of the elbow shown in figure 1. Assuming a steady incompressible flow and neglecting interphase mass transfer and surface tension, the one-dimensional mass and momentum conservation equations can be written, respectively, as (Hancox *et al.* 1980)

$$\frac{\partial}{\partial x}(\alpha_k u_k) = 0, \qquad [3]$$

$$\alpha_k \rho_k \bar{u}_k \frac{\partial \bar{u}_k}{\partial x} + \alpha_k \frac{\partial \bar{P}_k}{\partial x} - (P_i - \bar{P}_k)\frac{\partial \alpha_k}{\partial x} = -\tau_{wk} - \tau_{ik} - \alpha_k \rho_k g \sin\phi, \qquad [4]$$

where x is the distance from C, $\bar{P}_k$ is the pressure in the bulk phase k, P_i is the interface pressure, and τ_{wk} and τ_{ik} denote the force acting on phase k per unit flow volume due to wall shear and interfacial shear, respectively, and ϕ is the upward inclination of the pipe. The overbars refer to phase-average quantities, defined by

$$\bar{a}_k = \frac{1}{A_k}\int_{A_k} a_k \, dA,$$

where A_k is the portion of the pipe area occupied by phase k.

Equation [4] can be transformed to a more convenient form if the reasonable assumption is made that the pressure variation over the cross section of each phase is due to hydrostatic forces only. It then follows that

$$\bar{P}_k = P_i + \rho_k g (y_i - \bar{y}_k), \qquad [5]$$

where y_i is the elevation of the interface, and $\bar{y}_k$ the elevation of the centroid of A_k, both referred to an arbitrary datum. $\bar{y}_k$ is given by

$$\bar{y}_k = \frac{1}{A_k}\int_{A_k} y \, dA. \qquad [6]$$

Substituting [5] into [4], and using [6], the momentum equation for phase k becomes

$$\alpha_k \rho_k \bar{u}_k \frac{\partial \bar{u}_k}{\partial x} + \alpha_k \frac{\partial P_i}{\partial x} + \frac{A}{S_i}(-)^k \alpha_k \rho_{ki} g \frac{\partial \alpha_k}{\partial x} = -\tau_{wk} - \tau_{ik} - \alpha_k \rho_k g \sin\phi, \qquad [7]$$

where S_i is the interface width (see figure 2), A is the duct area, and

$$(-)^k = \begin{cases} -1 & \text{for } k = G, \\ +1 & \text{for } k = L. \end{cases}$$

Note the [7] is applicable to a duct of arbitrary constant cross section.

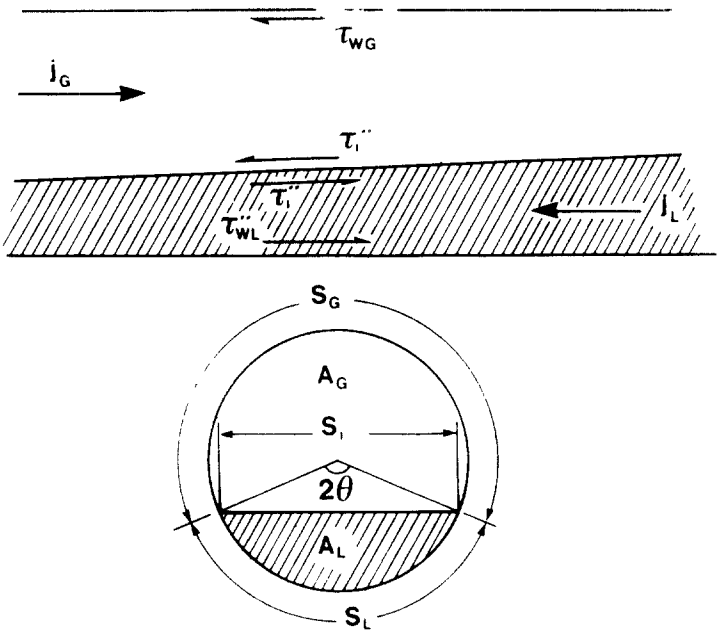

Figure 2 Stratified flow geometry

The momentum source terms τ_{wk} and τ_{ik} can be expressed in terms of friction factors. By geometry we have, referring to figure 2,

$$\tau_{wg} = -|\tau_{wg}''|\frac{S_G}{A}, \tau_{wl} = |\tau_{wl}''|\frac{S_L}{A} \quad [8]$$

and

$$\tau_{ig} = -\tau_{il} = -\tau_i''\frac{S_i}{A} \quad , \quad [9]$$

where S_k denotes the tube perimeter in contact with phase k, S_i is the interface width, and τ_{wk}'' and τ_i'' are the wall and interfacial shear stresses, respectively.

The wall stresses are expressed in terms of smooth-tube friction factors f_{wk} as

$$|\tau_{wk}''| = \frac{1}{2}f_{wk}\,\rho_k\,\bar{u}_k^2\,, \quad [10]$$

where

$$f_{wG} = C_G\,\mathrm{Re}_G^{-n}, \quad f_{wL} = C_L\mathrm{Re}_L^{-m}\,. \quad [11]$$

Note that $\bar{u}_k$ in [10] is the actual phase velocity rather than the superficial velocity. For turbulent flow we use coefficients $C_G = C_L = 0.046$, $n = m = 0.2$; for laminar flow we use $C_G = C_L = 16$, $n = m = 1$. Following Agrawal *et al.* (1973) the Reynolds numbers are defined by

$$\mathrm{Re}_k = \frac{\bar{u}_k D_{Ek}}{\nu_k}\,,$$

where ν_k is the kinematic viscosity of phase k, and the D_{Ek} are hydraulic diameters defined by

$$D_{EG} = \frac{4A_G}{(S_G + S_i)},$$
$$D_{EL} = \frac{4A_L}{S_L}. \qquad [12]$$

As a first approximation the interface is assumed to be hydrodynamically smooth, and the interfacial shear stress is taken as being roughly equal to the shear stress at the wall in the part of the duct occupied by the gas phase, i.e. $\tau_i'' = \tau_{wG}''$. A similar assumption was made by Taitel & Dukler (1976) in their analysis of flow regime transitions in cocurrent stratified flow. The effect of using other formulations for interfacial shear is discussed in section 3.5 below.

Using the fact that $\alpha_G + \alpha_L = 1$, the conservation equations [3] and [7] can be solved for the derivatives $\partial\alpha_G/\partial x$, $\partial P_i/\partial x$, $\partial \bar{u}_G/\partial x$, and $\partial \bar{u}_L/\partial x$. If for the moment we restrict our attention to the case of turbulent gas-turbulent liquid flow, so that $C_L = C_G = 0.046$, $n = m = 0.2$, the void fraction gradient can be written in nondimensional form, using [10]–[12], as

$$\frac{1}{(\mathrm{Re}^{*-n})}\frac{d\alpha_G}{d\tilde{x}} = \left\{\frac{2C_G}{\pi}\left[\left(\frac{\pi}{\tilde{S}_G + \tilde{S}_i}\right)^{-n}(\tilde{S}_i + \alpha_L\tilde{S}_G)\frac{j_G^{*2-n}}{\alpha_G^2} + K^{-n}\left(\frac{\pi}{\tilde{S}_L}\right)^{-n}\alpha_G\tilde{S}_L\frac{j_L^{*2-n}}{\alpha_L^2}\right] + \alpha_l\alpha_g I\right\} \Big/ \left\{\frac{\pi\alpha_L\alpha_G}{4\tilde{S}_i} - \frac{\alpha_L}{\alpha_G^2}j_G^{*2} - \frac{\alpha_G}{\alpha_L^2}j_L^{*2}\right\}, \qquad [13]$$

where

$$C_G = 0.046, n = 0.2$$

and

$$\mathrm{Re}^* = \frac{D}{\nu_G}\sqrt{\frac{gD(\rho_L - \rho_G)}{\rho_G}}, \qquad [14]$$

$$K = \frac{\nu_G}{\nu_L}\sqrt{\frac{\rho_G}{\rho_L}}, \qquad [15]$$

$$I = \mathrm{Re}^{*n}\sin\phi, \qquad [16]$$

and $\tilde{x} = x/D$, etc. Referring to figure 2, the nondimensional perimeters and the void fraction can be expressed in terms of the angle θ (radians) using

$$\tilde{S}_G = \pi - \theta, \tilde{S}_L = \theta, \tilde{S}_i = \sin\theta,$$
$$\alpha_G = 1 - \frac{1}{\pi}(\theta - \frac{1}{2}\sin 2\theta). \qquad [17]$$

Using [17], $\tilde{S}_G$, $\tilde{S}_L$, and $\tilde{S}_i$ can be expressed as functions of α_G only.

Critical velocity. It is seen from [13] that $d\alpha_G/dx \to \infty$ when α_G satisfies the equation

$$\frac{\pi\alpha_L\alpha_G}{4\tilde{S}_i} - \frac{\alpha_L}{\alpha_G^2}j_G^{*2} - \frac{\alpha_G}{\alpha_L^2}j_L^{*2} = 0. \qquad [18]$$

For $j_G^* = 0$, this reduces to

$$j_L^* = \sqrt{\frac{\pi \alpha_L^3}{4\tilde{S}_i}},$$

which for $\rho_G << \rho_L$ is the same as

$$u_L = \sqrt{\frac{gA}{S_i}}. \qquad [19]$$

Equation [19] is the classical equation for the critical velocity in a channel of arbitrary cross section (Chow 1959). Since the condition $(d\alpha_G/dx) \rightarrow \infty$ can be applied at the pipe exit in a free out-fall, the two-fluid formulation thus correctly describes the exit conditions in this case. Inclusion of the term in j_G^* in [18] shows how the exit (critical) depth is modified by a countercurrent gas flow; this correction is not normally accounted for in open channel flow analysis.

In the following we will assume that the critical flow condition [18] is satisfied in the pipe exit plane at E. It should be noted that this assumption introduces some error. In actual fact, because of two-dimensional effects, the critical velocity in a round pipe does not occur exactly at the end of the pipe, but rather one or two diameters upstream (see Smith (1962). For present purposes, since we are considering pipes with a large length-to-diameter ratio, that correction to the one-dimensional theory will be ignored.

3.3 Calculation of flooding curve

Equation [13] can be written as

$$\frac{1}{(\mathrm{Re}^{*-n})} \frac{d\alpha_G}{d\tilde{x}} = f(\alpha_G, j_L^*, j_G^*, K, I). \qquad [20]$$

Referring to figure 1, [20] can be integrated between the hydraulic jump C and the exit E to give

$$\lambda = \frac{L(\mathrm{Re}^{*-n})}{D} = \int_{\alpha_{Gi}}^{\alpha_{Go}} \frac{d\alpha_G}{f(\alpha_G, j_L^*, j_G^*, K, I)}, \qquad [21]$$

where L is the distance CD (identified with the length of the lower limb of the elbow) and the subscripts o and i refer to conditions at the pipe exit (critical plane) and at the crest of the hydraulic jump, respectively.

Now [1] provides a relationship between α_{Gi} and j_G^* just before flooding inception and [18] relates α_{Go} to j_G^* and j_L^*. Thus [1], [18], and [21] give a relationship between j_G^* and j_L^* at flooding, in terms of the nondimensional parameters λ, I, and K, where λ is a modified length-to-diameter ratio for the lower limb of the elbow defined by [21], I is an inclination parameter defined by [16], and K is a nondimensional group depending only on fluid properties defined by [15]. Values of K for some common two-phase mixtures are listed in table 1.

The solution of these equations was calculated numerically for different combinations of λ, K, and I. The steps in the solution were as follows:

(i) calculate particular values for λ, K, and I appropriate to system of interest;
(ii) postulate j_L^*;
(iii) guess the value of j_G^* that would give flooding at the chosen value of j_L^*;
(iv) calculate α_{Gi} using [1] (with $j_{Gc}^* = 0.2$);
(v) calculate α_{Go} by iterative solution of the critical depth equation [18];
(vi) calculate the integral in [21] numerically using Simpson's Rule (a twenty step integration was used). This gives the value of λ compatible with the selected values of j_G^* and j_L^*;

Table 1. Values of K for various two-phase mixtures

Two-phase mixture				K
Air–water	(T = 25°C	P =	100 kPa)	0.61
Steam–Water	($T = T_{SAT}$	P =	100 kPa)	1 73
Steam–Water	($T = T_{SAT}$	P =	5 0 MPa)	0.47
Freon 113	(T = 25°C	P =	saturation pressure)	0.33
Freon 12	(T = 25°C	P =	saturation pressure)	0.41

(vii) repeat steps (ii)–(vi) until the calculated λ from step (vi) agrees with the actual value imposed in step (i) to within 0.1%.

3.4 Numerical results

(a) Horizontal lower limb. We first consider the case where the lower limb of the elbow is perfectly horizontal ($I = 0$). Numerical results are displayed in figure 3. These calculations are for a turbulent gas-turbulent liquid conditions ($n = 0.2$, $C_G = C_L = 0.046$). The range of K values covered embraces many two-phase flows of common interest (see table 1). The effect of the K parameters is seen to be only weak.

Over the parameter range shown in figure 3,

$$1 < \lambda < 16,$$

$$0.5 < K < 1.8,$$

$$0 < j_L^{*1/2} < 0.6,$$

the flooding curves can be represented with reasonable accuracy by the convenient equation

$$j_G^{*1/2} = 1.444 - 0.004\,\lambda - \cosh\left(\lambda^p K^q \left(j_L^{*1/2}\right)^r\right), \qquad [22]$$

where

$$p = 0.057,\ q = -0.020,\ r = 0.70\,.$$

The RMS error in $j_G^{*1/2}$ obtained by using [22] instead of the numerical results is under 2%. This equation can therefore be regarded as a physically based flooding correlation for countercurrent gas–liquid flow in a horizontal-to-vertical pipe elbow.

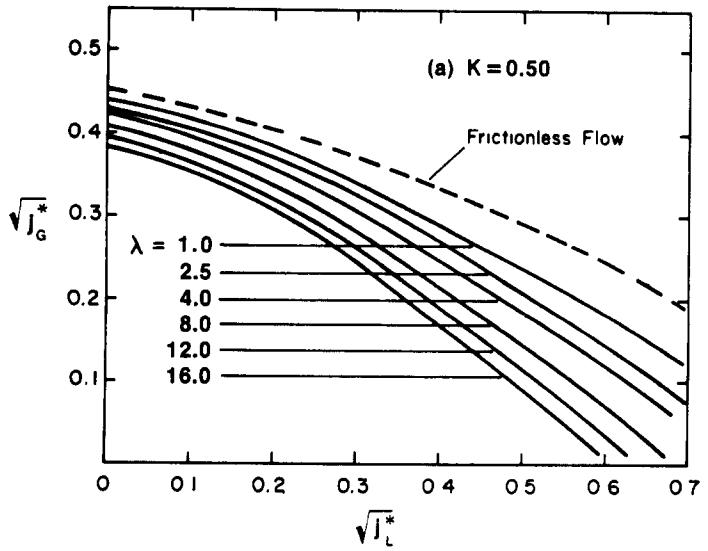

Figure 3a

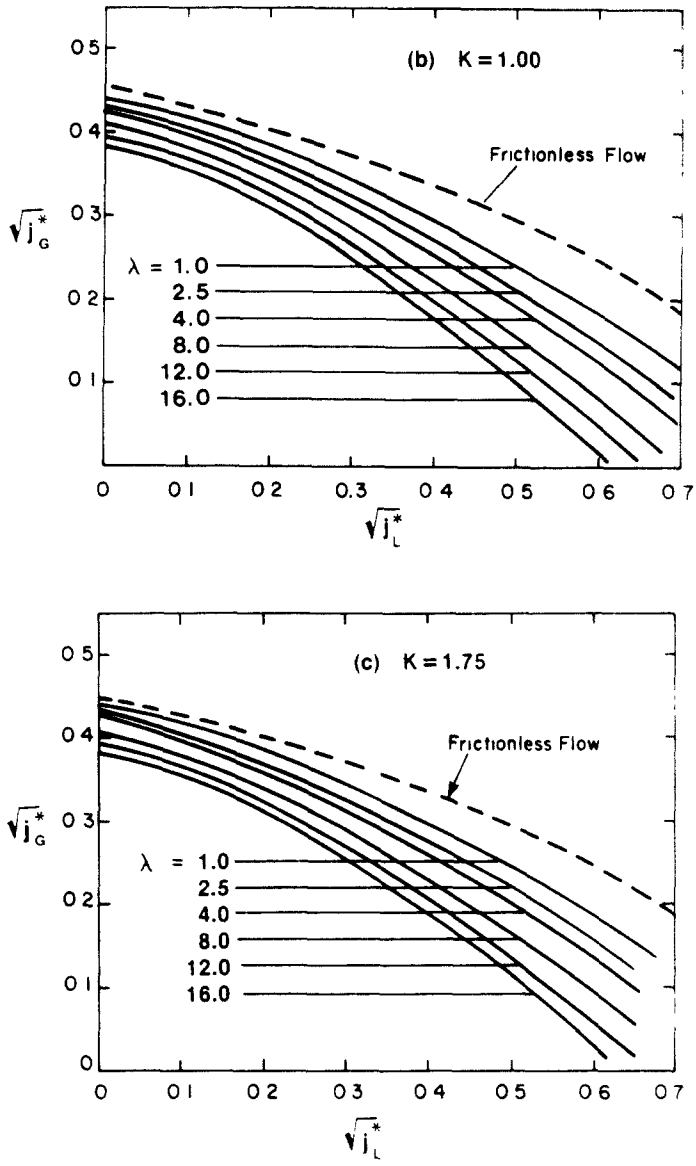

Figures 3b,c

Figure 3 Calculated flooding curves for turbulent gas-turbulent liquid flow Vertical-to-horizontal elbow.

An interesting limiting case is that of an ideal frictionless in the vertical-to-horizontal elbow. For this case $\alpha_{Gi} = \alpha_{Go}$, and the flooding curve is obtained simply by eliminating α_G between [1] and [18]. For $0 < j_L^* < 0.9$, the flooding curve thus obtained is described accurately by the quadratic fit:

$$j_G^{*1/2} = 0.447 - 0.176 j_L^{*1/2} - 0.263 j_L^* , \qquad [23]$$

which is, of course, independent of λ and K. Equation [23] is plotted in figure 4 as the line marked "frictionless flow". It is seen that friction has a significant effect on the flooding limit for the cases shown.

(b) Upwardly inclined lower limb. The effect of a small upward inclination of the lower limb of the elbow is to increase the upward slope of the liquid interface in the direction of the hydraulic jump. Since for given values of j_L^* and j_G^* the liquid depth at E is fixed at the critical depth (obtained by solving [18]) the steepening of the interface slope causes an increase in the height of the hydraulic jump; the consequence is a reduction in the gas flow rate needed to cause flooding.

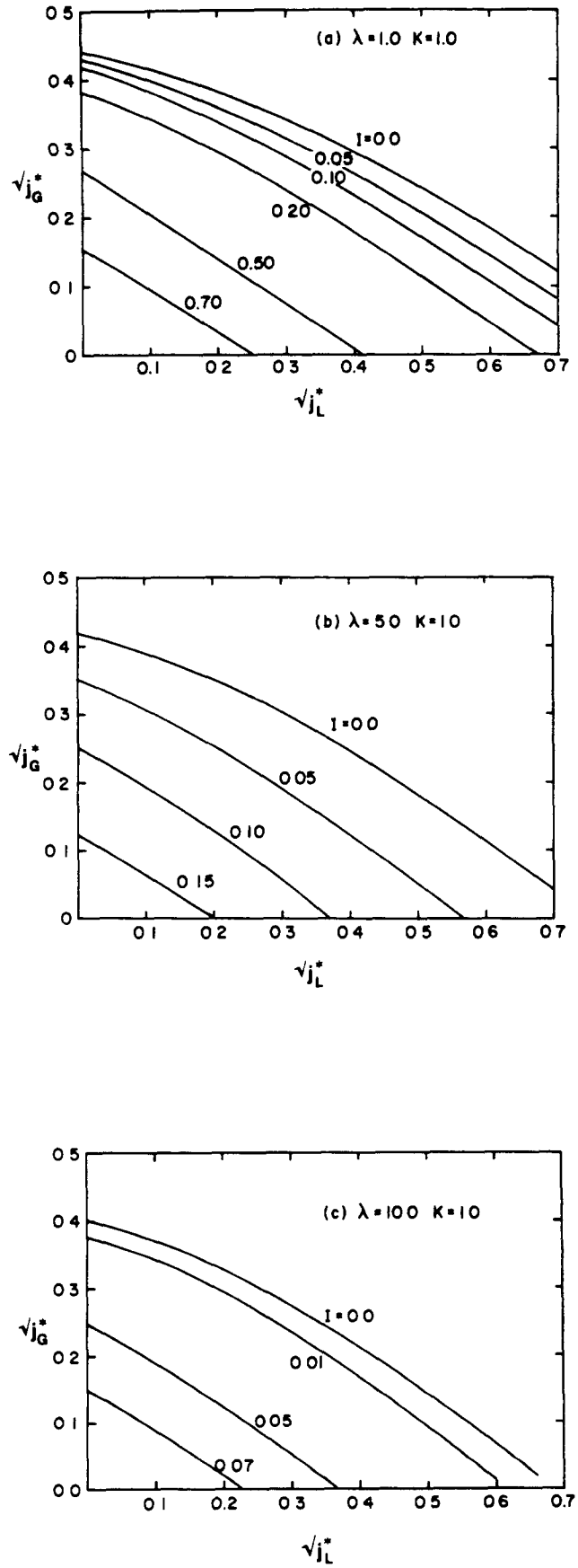

Figure 4. Effect of upward inclinations on flooding curve for different length-to-diameter ratios.

Results of numerical calculations for different values of the inclination parameter I (> 0), are given in figure 4. Again the calculations assume turbulent gas-turbulent liquid flow. The results are all for $K = 1.0$, but the curves are reasonably accurate for the range of K values in table 1. It should be noted that all the calculations assume that the condition for slugging at the hydraulic jump is given by [1], i.e. that the instability condition is the same in an inclined pipe as in a horizontal pipe.

It can be seen that small upward inclinations have a marked effect on the predicted flooding curve, particularly for large values of the length parameter λ (note that for 25°C air–water flow in a 50 mm diameter pipe a value of I of 0.5 corresponds to an upward inclination on only 3.4°). As the inclination is increased the maximum liquid downflow that can be achieved for a given gas upflow decreases further and further. Eventually a threshold inclination is predicted where complete liquid carry-up ($j_L^* = 0$) occurs even in the limit where gas flow rate approaches zero, $j_G^* \to 0$, implying that countercurrent flow is now impossible. Physically, this threshold upward inclination corresponds to the point at which the slope of the interface is such that the liquid bridges the pipe at C, even in the absence of gas flow. By making the substitutions $j_G^* = j_L^* = 0$, $\alpha_{Go} = 1$, $\alpha_{Gi} = 0$ in [21] and [13] this critical inclination is calculated as

$$I = \frac{1}{\lambda} \text{ or } \sin\phi = \frac{D}{L}, \qquad [24]$$

which is the result that one also obtains from simple geometrical arguments.

(c) Downwardly inclined lower limb. The effect of a downward inclination of BE ($I < 0$) is to reduce the height of the hydraulic jump. Beyond a threshold value of the downward inclination (typically less than 0.5°) [13] predicts that $d\alpha_g/d\tilde{x}$ becomes negative in subcritical flow, implying that the approach to critical flow at E cannot occur. The only physically meaningful solution now is one where the liquid velocity is supercritical everywhere in the lower limb of the elbow, implying that a hydraulic jump cannot exist.

Since flooding in an elbow with a downwardly inclined lower limb in which there is supercritical flow has not been studied experimentally in any detail, no theoretical analysis of this interesting case is attempted herein. It should be noted however that the present model, which assumes a subcritical flow in the lower limb of the elbow, is not applicable for this case.

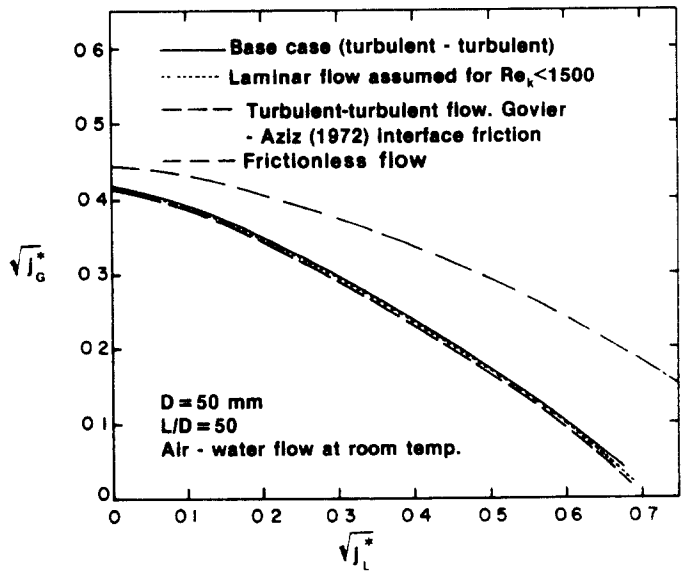

Figure 5. Sensitivity of flooding curve to variations in interfacial friction modeling.

3.5 Effect of different assumptions about interfacial shear

The above calculations are all for a turbulent gas-turbulent liquid flow where the interface shear stress is equal to the wall shear stress in the gas phase. In practice laminar flow would be expected in the limits $j_L^* \to 0$ and $j_G^* \to 0$, and it is interesting to examine the effect this will have on the predicted flooding curves. Figure 5 shows a particular example of atmospheric pressure air-water flow in a 50 mm diameter vertical-to-horizontal elbow with $D = 50$ mm, $L/D = 50$ (corresponding to $K = 0.61$, $\lambda = 5.45$, $I = 0$). The flooding curve predicted using the turbulent–turbulent assumption is shown as the solid line. The dotted line is the curve obtained by allowing the friction factors to transition to laminar flow values for $\mathrm{Re}_k \leqslant 1500$. It is seen that ignoring the transition to laminar flow makes very little difference to the calculated flooding curve.

We have also investigated the effect of using different formulations for the interfacial friction factor. Govier & Aziz (1972) recommended that for cocurrent stratified flow with a smooth interface, the interfacial shear stress can be calculated from the formulae

$$\tau_i'' = \frac{1}{2} f_i \rho_G \bar{u}_G^2, \quad f_i = 1.29\, \mathrm{Re}_G^{-0.57}, \qquad [25]$$

where f_i denotes the interface friction factor. The flooding curve calculated using [25] is shown as the broken line in figure 5. Again it is seen that this refinement in the calculation of τ_i'' has a negligible effect on the predicted flooding curve. The flooding curve for frictionless flow [23] is also included in figure 5. It is seen that interface and wall friction have a significant effect on the flooding limit for the example shown.

4. COMPARISON WITH EXPERIMENTAL DATA

In part I we described measurements of countercurrent flooding limits for atmospheric pressure air–water flow in several horizontal-to-vertical pipe elbows. Limited data were also presented where the lower limb of the elbow was upwardly or downwardly inclined. The range of tube geometries used in the tests were

$$\begin{gathered} 36\ \mathrm{mm} \leqslant D \leqslant 47\ \mathrm{mm}, \\ 24 \leqslant L/D \leqslant 95, \\ 0 \leqslant R_c \leqslant 300\ \mathrm{mm}, \\ -0.6^\circ \leqslant \phi \leqslant 0.6^\circ, \end{gathered}$$

where D and L/D denote the tube diameter and length-to-diameter ratio of the horizontal leg, respectively, and R_c is the radius of curvature of the elbow.

Representative data for the horizontal-to-vertical elbows ($\phi = 0$) are compared with predictions of the present theory in figures 6–8. The predictions are shown as bands to reflect the experimental uncertainty in the true inclination of the lower limb of the elbow, estimated as $\pm$ 0.03° (the upper and lower edges of the bands correspond to the flooding curves predicted assuming an inclination of −0.03° and + 0.03°, respectively). Overall agreement is reasonable, and the gas flow for complete liquid carry-up ($j_L^* = 0$) is quite well predicted. The main discrepancies are the underprediction of flooding limit for the shorter tube lengths, $L/D < 30$ (see figure 7), and the failure of the model to account for the observed effect of R_c on the flooding limit. The errors are probably due mainly to the use of [1], with $j_{Gc}^* = 0.2$, to describe the onset of slugging at the hydraulic jump. It is seen from an examination of the data in part I that j_{Gc}^* varies between 0.15 and 0.25 for the experimental conditions and this variation could easily explain the discrepancies. In practice j_{Gc}^* probably depends on the shape of the hydraulic jump, which in turn, is influenced by the geometry of the pipe, and in particular the shape of the bend. However, no attempt has been made as part in this investigation, to correlate the effective value of j_{Gc}^* with system geometry.

Figure 9 shows a comparison with the limited data given in part I where the lower

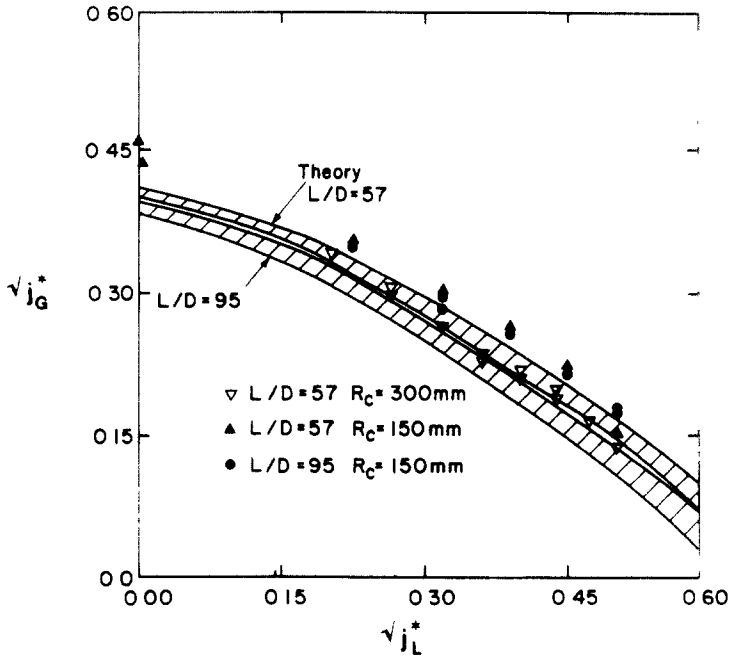

Figure 6. Comparison with data for rounded elbows with different L/D ratios (D = 35 5 mm).

limb of the elbow was initially inclined. The model predictions are again shown as bands, reflecting the $\pm$ 0.03° experimental uncertainty in the inclination. The experimental trends are seen to be quite well represented by the theory, although additional data are obviously needed to confirm this agreement. For the case where the lower limb of the elbow is downwardly inclined (upper curve in figure 9) the present model becomes invalid for $j_L^{*1/2} > 0.2$, when a transition to supercritical flow is predicted (see section 3.4(c) above).

Krowlewski (1980) reported measurements of flooding limits for air–water flow in a horizontal tube connected at inlet to a 90° vertical elbow. In her tests the tube dimensions were D = 51 mm, L/D = 11.5. The onset of flooding was taken as the point at which

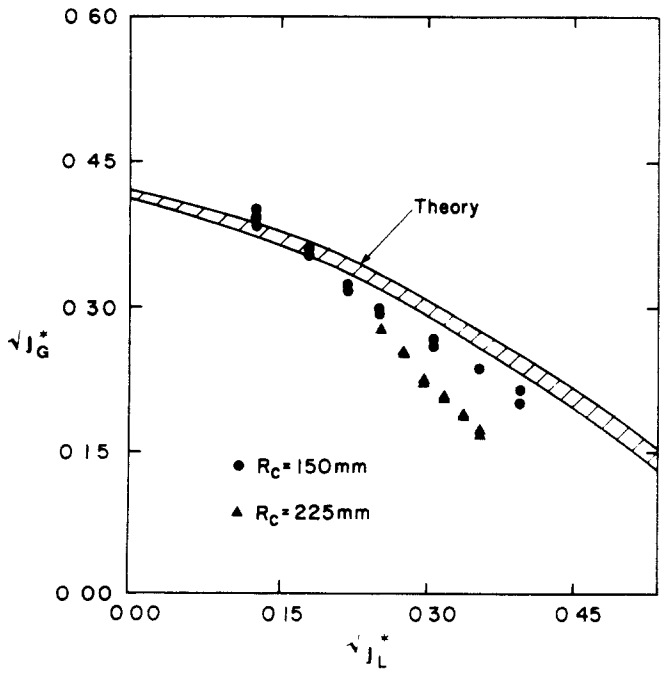

Figure 7 Comparison of theory with data for different radius of curvature values (L/D = 47, D = 44.0 mm)

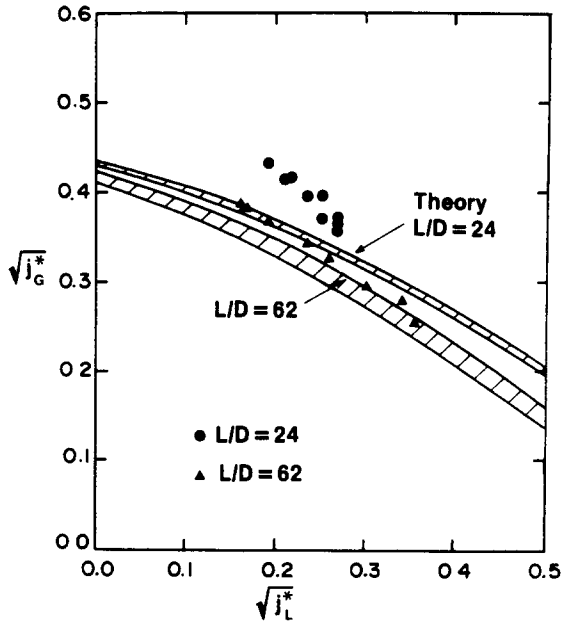

Figure 8. Comparison of theory with data for square elbow, $R_c = 0$, $D = 44.0$ mm.

the pressure drop across the test section increased sharply as the gas flow rate was gradually increased. Three geometrical configurations were used, as illustrated in figure 10.

Krowlewski's data are plotted in figure 11. There is a noticeable difference between data for configuration A and data for configurations B and D, indicating that the flooding limit is sensitive to details of the horizontal leg exit geometry. This effect was also noted in our experiments described in part I and is believed due to the influence of exit geometry on critical exit depth. Predictions of the theory are also shown in figure 11. Agreement for configurations B and D is reasonable, but the gas flow rate required for flooding in configuration A is over predicted. The fact that the best agreement is obtained for cases B and D is not surprising, since the exit conditions in these cases correspond most closely to the free out-fall condition assumed in the model.

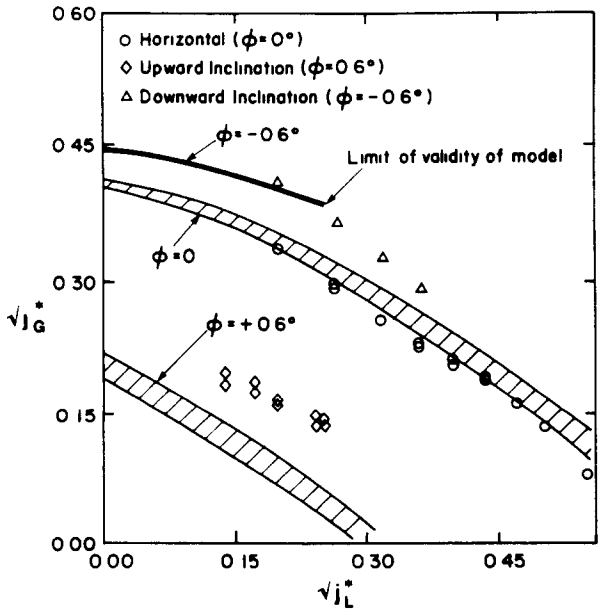

Figure 9. Comparison of theory with data showing effect of inclination (theory and data for $L/D = 57$, $D = 36.5$ mm).

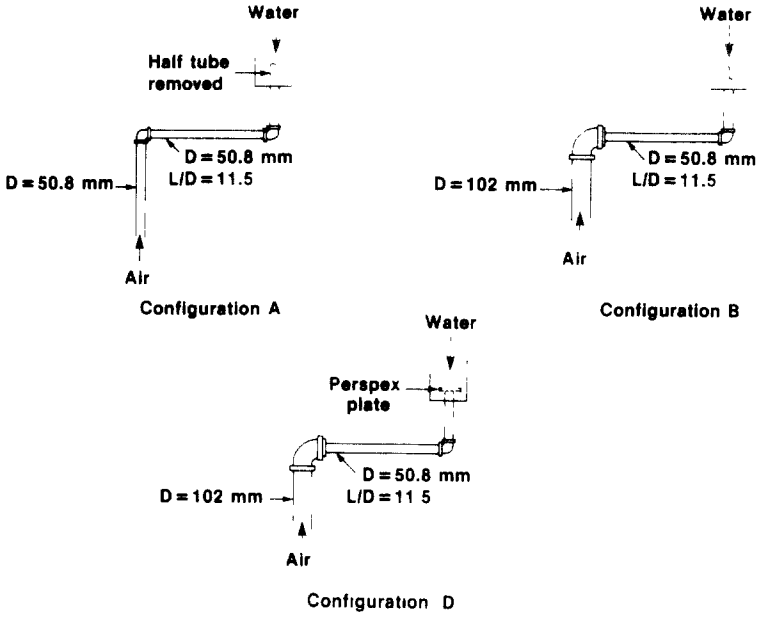

Figure 10. Apparatus used in the experiments of Krowlewski (1980).

5. COMPARISON WITH OTHER FLOODING MODELS

Figure 12 compares predictions of the present model with those of the Wallis (1969) correlation for a vertical tube (sharp-edged entry) and those of the Gardner (1983) model for a horizontal tube. The calculations are for an air–water flow in a tube with $D = 36.5$ mm, $L/D = 57$. Also shown are the experimental data for this case taken from figure 6. It is seen that the air flow required to produce flooding in a horizontal tube is much smaller than the air flow predicted for an equivalent vertical tube, using the Wallis correlation. The Gardner model predicts a lower flooding limit over part of the range, but does not agree well with the data. Also, this model predicts that the air flow rate for complete carry-up ($j_L^* = 0$) is close to $j_G^* = 1.1$, whereas the data show that complete liquid carry-up occurs at $j_G^* \simeq 0.2$, representing a major discrepancy. The present model reproduces the data trend fairly well, and gives the complete carry-up limit with reasonable accuracy.

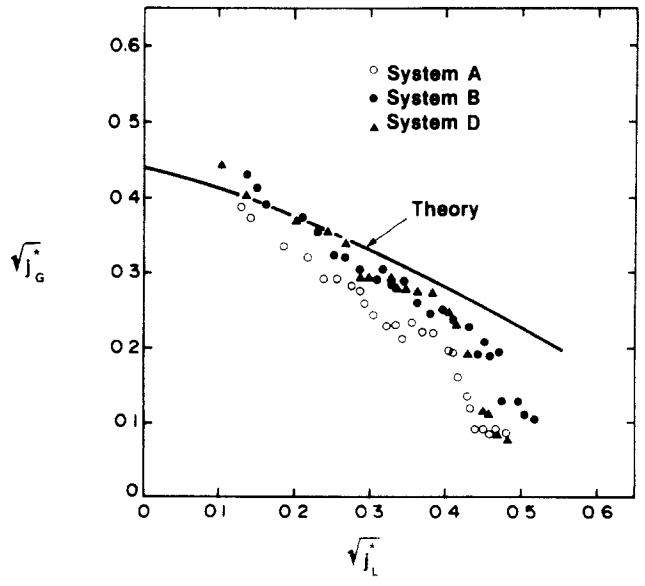

Figure 11 Comparison of theory with data of Krowlewski (1980) ($D = 51$ mm, $L/D = 11.5$)

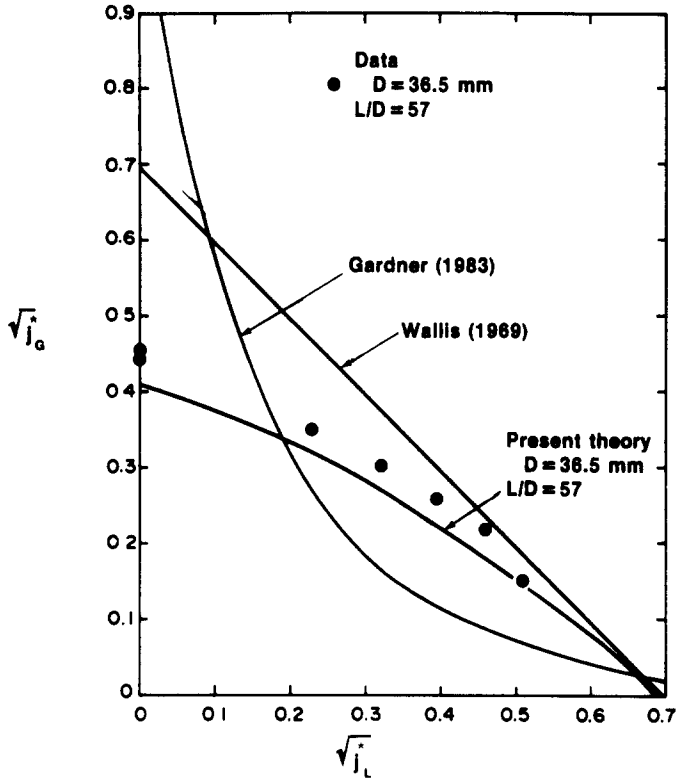

Figure 12. Comparison of various flooding models.

6. CONCLUSIONS

A theoretical model has been developed to predict the flooding limit in a pipe elbow of which the upper limb is vertical and the lower limb is horizontal or inclined slightly. The model assumes that prior to flooding, a smooth stratified flow exists in the lower limb of the elbow. A free out-fall is assumed at the exit where the liquid velocity is equal to the critical velocity for open-channel flow. Flooding is assumed to occur because of the formation of unstable waves (slugging) at the crest of a hydraulic jump located in the lower limb of the elbow close to the bend. The flooding curve is calculated by solving for the stratified two-phase flow in the lower limb of the elbow.

The model has been used to develop a generalized flooding curve for a horizontal-to-vertical elbow in terms of nondimensional parameters. Calculated flooding limits for an elbow where the lower limb is upwardly inclined have been presented in graphical form.

The theory has been found to give a reasonable representation of available flooding data for elbows. In particular the observed trends with respect to the length and inclination of the lower limb of the elbow are quite well described. The model appears to be a significant improvement over alternative methods for predicting flooding in pipe geometries of this kind.

Acknowledgments —Parts of this work were supported by the US National Science Foundation under Grant CPE 81-12667.

REFERENCES

AGRAWAL, G. C., GREGORY, G. A. & GOVIER, G. W. 1973 An analysis of horizontal stratified two-phase flow in pipes. *Can. J. Chem. Eng.* **51**, 280–286.

CHOW, V. T. 1959 *Open Channel Hydraulics*, Chap. 3. McGraw-Hill, New York.

GARDNER, G. C. 1983 Flooded countercurrent two-phase flow in horizontal tubes and channels. *Int. J. Multiphase Flow* **9**, 367–382.

GOVIER, G. W. and AZIZ, K. 1972 *Flow of Complex Mixtures in Pipes*. Van Nostrand-Reinhold, New York.

HANCOX, W. T., FERCH, R. L., LIU, W. S. & NIEMAN, R. E. 1980 One-dimensional models for transient gas–liquid flows in ducts. *Int. J. Multiphase Flow* **6**, 25–40.

KROWLEWSKI, S. M. 1980 Flooding limits in a simulated nuclear reactor hot-leg. Massachusetts Institute of Technology, B.Sc. Thesis.

RICHTER, H. J., WALLIS, G. B., CARTER, K. H. & MURPHY, S. L. 1978 De-entrainment and countercurrent air–water flow in a model PWR hot-leg. U. S. Nuclear Regulatory Commission Report NRC-0193-9

SIDDIQUI, H., ARDRON, K. H. & BANERJEE, S. 1986 Flooding in an elbow between a vertical and a horizontal or near horizontal pipe. Part I: Experiments. *Int. J. Multiphase Flow* **12**, 531–541.

TAITEL, Y. & DUKLER, A. W. 1976 A model for predicting flow regime transitions in horizontal and near horizontal gas–liquid flow. *AIChE J.* **22**, 19–55.

WALLIS, G. B. 1969 *One-dimensional Two-Phase Flow*, Chap. 6. McGraw-Hill, New York.

WALLIS, G. B. & DOBSON, J. E. 1973 The onset of slugging in horizontal stratified air–water flow. *Int. J. Multiphase Flow* **1**, 173–193.